

## Periodic Pattern Inspection using Convolution Masks

Y. S. Weng

M. H. Perng

Department of Power Mechanical Engineering, National Tsing Hua University,  
101 Sec. 2, Kungfoo Rd., 300, Hsinchu, Taiwan, R. O. C.

### Abstract

A two-dimensional (2-D) convolution mask is proposed for detecting the location of irregularities and defects in a periodic two-dimensional signal or image. In this approach, defects on a 2-D test image is automatically filtered out by a 2-D convolution mask implementing the spatial filter. This approach is reliable and computationally efficient. Besides, unlike the traditional die-to-die approach, it can avoid all troubles in a database image, a scaling or alignment procedure.

### 1. Introduction

Inspection of defects on a two-dimensional periodic pattern inspection occurs to a wide range of industrial problems including defect detection of memory chips, shift registers, switched capacitors, CCD arrays, LCD displays and other areas.

The die-to-die inspection method [1-6] has been adopted in many industrial applications for its simplicity and computational efficiency. However, this approach may require precise alignment and segmentation of repeated patterns [4-6], and the required precisions increase with the density of the repeated pattern. These steps can be quite sophisticated and computationally demanding [3, 6] owing to the fact that the size of the defects is becoming smaller, and harder to detect.

On the other hand, filtering techniques have a very good potential in avoid difficulties encountering in registration, segmentation and building golden template. Since periodic pattern is a special case of structured textures, the inspection techniques originally developed for structured textures can also be applied to periodic patterns. For instance, the wavelet transform [7-8] and the Gabor filter [9-10] have been applied to texture defect detection. Unfortunately, both of them are computationally demanding.

Discrete Fourier transform demands less computation effort and has been applied to defect detections [11-13]. However, both forward and inverse discrete Fourier transforms still require considerable computation time, which is not suitable for industries such as LCD displays manufacture.

In this paper, it proposes a two-dimensional convolution mask for the inspection of periodic patterns. This approach has two advantages: (1)Its total computation effort is of the same order of the basic die-to-die inspection method. (2)It can sharply detect defected areas.

### 2. Reconstructing periodic patterns using ideal band-pass filters

In this section, first the characteristics of a periodic pattern and various types of defected area in the frequency domain will be discussed. Based on these discussions, an ideal multi-band filter will be proposed in the frequency domain to sharply reconstruct a periodic pattern.

#### 2.1 2-D Fourier transform of a continuous image

Let  $x$ , and  $y$  be the spatial coordinates of a continuous image,  $f(x, y)$  be a periodic pattern, where  $x$ , and  $y$  are real numbers, while  $p(x, y)$  be the unit pattern defined in the interval  $x \in [0, T_x]$ ,  $y \in [0, T_y]$  and  $p(x, y)$  repeats itself in  $f(x, y)$ , that is

$$f(x, y) = p(\bar{x}, \bar{y}) \quad (1)$$

if and only if  $x = \bar{x} + nT_x$  and  $y = \bar{y} + mT_y$ , where  $n$  and  $m$  are integers,  $T_x$  and  $T_y$  are spatial periods. Let

$$\psi(x, y) = \sum_{m=-\infty}^{\infty} \sum_{n=-\infty}^{\infty} \delta(x - nT_x) \delta(y - mT_y)$$

be a 2-D comb function. Then,  $f(x, y)$  can be expressed as the unit pattern  $p(x, y)$  convoluted with the comb function  $\psi(x, y)$

$$f(x, y) = p(x, y) \otimes \psi(x, y) \quad (2)$$

where  $\otimes$  denotes the convolution operation. Finally, let  $F(u, v)$  and  $P(u, v)$  be, respectively, the Fourier transforms of  $f(x, y)$  and  $p(x, y)$ , it can be shown by using the convolution theorem [6] that

$$F(u, v) = P(u, v) \bullet \bar{\psi}(u, v) \quad (3)$$

where  $\bar{\psi}(u, v)$  is the Fourier transform of  $\psi(x, y)$ ,

$$\bar{\psi}(u, v) = \sum_{m=-\infty}^{\infty} \sum_{n=-\infty}^{\infty} \delta(u - n\omega_x) \delta(v - m\omega_y) \quad (4)$$

and

$$\omega_x = 2\pi/T_x, \quad \omega_y = 2\pi/T_y \quad (5)$$

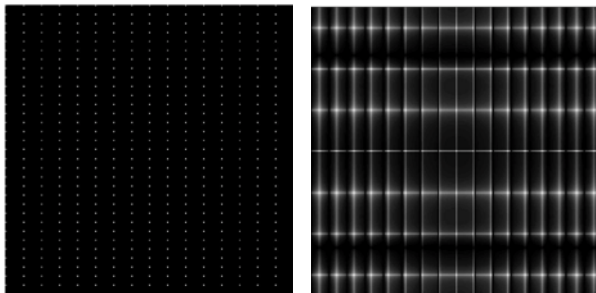
However, the simplicity of this relationship breaks when both  $f(x, y)$  and  $p(x, y)$  are two-dimensional discrete signals with finite window length mainly due to

the leakage effect as will be discussed in the following subsection.

## 2.2 2-D Discrete Fourier transform of an image

In most industrial applications such as the automatic optical inspection (AOI) or the automatic vision inspection (AVI), an image is captured by a charge-coupled device (CCD) using finite pixels, the two-dimensional (2-D) discrete Fourier transform (DFT) should be applied instead of the Fourier transform. In such a case, the previous statements basically hold true except that (1) aliasing may occur when the Nyquist sampling criterion fails, and (2) the leakage effect may occur due to finite sampling points.

However,, when the numbers of columns and rows, denoted as  $N_x$  and  $N_y$ , in a digital image periods happen to be the spatial periods  $T_x$  and  $T_y$  multiplied by some integers, the leakage effect is unobservable from the DFT of the image. Otherwise, the leakage effect could be significant.



(a)  $T_x=8, T_y=16$       (b)  $T_x=7, T_y=17$

Figure 1: gain plot of a periodic pattern

For instance, consider a digital image of a periodic pattern  $f^*(j,k)$ , where  $f^*(j,k)$  consists of  $N_x \times N_y = 256 \times 256$  pixels,

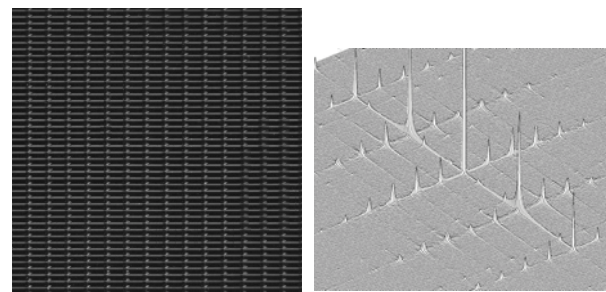
$$f^*(j,k) = \begin{cases} 1, & \text{for } j = nT_x \text{ and } k = mT_y \\ 0, & \text{otherwise} \end{cases} \quad (6)$$

$n, m = 0, 1, 2, 3, \dots$ , the periods are  $T_x=8$  pixels and  $T_y=16$  pixels. As is shown on Fig. 1(a), there is no leakage effect on the gain plot of the DFT of  $f^*(j,k)$  due to the fact that  $N_x = 32T_x$  and  $N_y = 16T_y$ .

However, when  $T_x=7$  pixels and  $T_y=17$  pixels, leakage occurs along both the horizontal and vertical directions in the gain plot of the DFT, as is shown in Fig. 1(b), since neither of  $N_x$  and  $N_y$  is an integer multiplied by their corresponding periods  $T_x$  and  $T_y$ .

It should be noted that, in many disciplines of signal processing, aliasing and leakage are treated as unwanted noise. However, in the case of AOI and AVI, since aliasing and leakage are part of a ‘normal image’, they

should not be filtered out in the process of building a ‘golden template’. For instance, Fig. 2 shows the original image of a ‘normal’ LCD panel in Fig. 2(a) and its spectrum in Fig 2(b), where the effect of leakage is obvious. The number of pixels in Fig. 2(a) is  $256 \times 256$  pixels, while the periods of the pattern are 6 pixels and 17 pixels along horizontal and vertical axis, respectively. Referring to Fig. 2(b), the height is the spectrum of the image in Fig. 2(a) at a location  $(u, v)$  in the frequency domain, the highest peak occurs at the location where  $(u, v) = (0, 0)$  and the height of this peak corresponds to the dc-bias or average intensity of the image in Fig. 2(a), while the locations  $(\bar{u}, \bar{v})$  where local peaks of the spectrum occur correspond to the sampling points where  $(\bar{u}, \bar{v}) = (n\omega_x, m\omega_y)$  with  $n$  and  $m$  being integers. The leakage effect is localized and decays rapidly away from the sampling points where  $(\bar{u}, \bar{v}) = (n\omega_x, m\omega_y)$ , but is not negligible.



(a) LCD array      (b) Spectrum of the LCD array  
 $f^*(j,k)$        $|F(u,v)| = |F\{f^*(j,k)\}|$

Figure 2: Spectrum and leakage of a LCD array

## 2.3 Pattern reconstruction via discrete Fourier transform

In this subsection an approach using the 2-D discrete Fourier transform will be presented for the reconstruction of a periodic pattern taking into account possible leakage in a ‘normal image’ so that it can sensitively and sharply discriminate the periodic pattern from defects with a minimal effect of blurring. Before that, existing approaches closest to the present one will be examined first.

The discrete Fourier transform has been applied to discriminate a defected textile from a good one by analyzing its frequency spectrum [11-13]. However, none of these works has ever attempted to determine the location and shape of defected areas, which is a must in the AOI and AVI industries.

There was, however, an attempt to pin-point the location and shape of defected areas in a periodic pattern [14] using the DFT, where a 2-D ideal low-pass filter has been designed to filter out defected areas. In this approach, first the DFT is applied to an image containing a periodic pattern, then a 2-D ideal low-pass filter is designed to filter out periodic patterns with the hope that only images of the defected areas will be left behind. And, finally, the inverse DFT is applied to recover the location and shape of

defected areas before applying a threshold to filter out noises in the spatial domain.

This approach, however, works only for very limited cases due to the following drawbacks. First, it implicitly assumes that there exists a radius on the frequency domain to separate the spectrum of defected areas in the low frequency range from that of the periodic pattern in the high frequency range. To meet this assumption, the size of defected areas must be sufficiently large, and the periodic pattern must have very strong contrast and/or a relatively small period. Otherwise, the spectrum of defected areas may seriously overlap with that of the periodic pattern causing difficulties in later steps for separating defected areas from the periodic pattern. Second, even in the cases where a radius barely exists to roughly separate defect areas from the periodic pattern, the boundary of defected areas will be blurred due to the low-pass filtering.

To amend the aforementioned drawbacks in order to propose an inspection technique that meets the more and more demanding need of AOI and AVI industries, the ideal multi-band filter  $|H_1(u, v)|$  shown in Fig. 3(b) is proposed to precisely and sharply reconstruct the periodic pattern from a defected image, and this filter will be implemented using a 2-D convolution mask in Section 3. Figure 3(a) is a 2-D representation of Fig. 2(b) where the intensity (grey level) at a frequency point  $(u, v)$  indicates the magnitude of the frequency spectrum. Fig. 3(b) shows the proposed ideal multi-band filter  $|H_1(u, v)|$  in the frequency domain whose value is binary, i.e., the value of the filter is 1 for all frequency points in the bright area and 0 for the rest in the dark area.

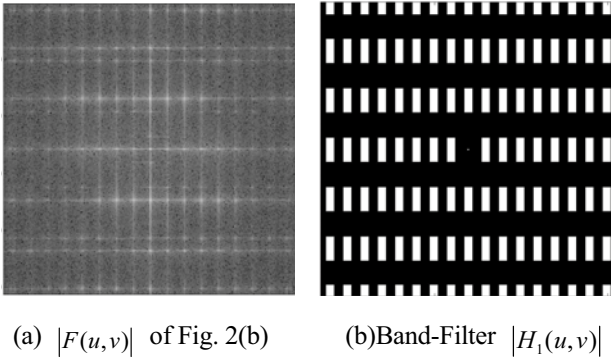


Figure 3: The proposed ideal multi-band filter

Please also notice that all bright areas (windows) are centered at the sampling points  $(\bar{u}, \bar{v}) = (n\omega_x, m\omega_y)$  to allow the passage of not only the ideal periodic pattern but also its leakage. However, no signal is allowed to pass in the lowest frequency range where the energy of defects dominates. Finally, once the periodic pattern is sharply reconstructed, the traditional golden template approach can be applied to detect defected areas.

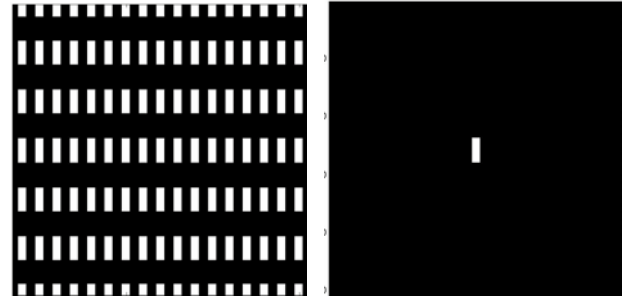
However, to speed up the inspection process, the ideal multi-band filter proposed in this section will be implemented as a 2-D spatial convolution mask to be detailed in Section 3 so that there is no need for the DFT and the inverse DFT.

### 3. Comb filter and the convolution mask

The ideal multi-band filter shown in Fig. 3(b) is difficult to implement by spatial convolution masks. However, it can be decomposed into two filters that can be easily implemented by spatial convolution masks.

Referring to Fig. 4, the ideal multi-band filter  $H_1(u, v)$  in the frequency domain can be decomposed into an ideal comb filter  $H_2(u, v)$ , an ideal low-pass filter  $H_3(u, v)$  and the dc-gain  $F(0, 0)$  of an image  $f^*(j, k)$ , that is

$$H_1(u, v) = H_2(u, v) - H_3(u, v) + F(0, 0) \quad (7)$$



(a) Ideal filter  $|H_2(u, v)|$  (b) Low-pass filter  $|H_3(u, v)|$

Figure 4: Decomposition of the ideal multi-band filter

The advantage with this implementation scheme lies in that the ideal comb filter  $H_2(u, v)$  can easily be obtained by the up-sampling of the ideal low-pass filter  $H_3(u, v)$  [15].

To approximate the non-causal ideal low-pass filter by a FIR filter, there exist many approaches [15]. To minimize the computation effort, the moving average filter [15] is applied in the paper to produce the results shown in Fig. 5(b).

Take the periodic pattern shown in Fig. 3(a) for instance, the bandwidths of the 2-D ideal low-pass filter  $H_3(u, v)$  are chosen as  $0.5\omega_x$  and  $0.5\omega_y$ , and a  $3 \times 3$  moving average filter is used to approximate the ideal low-pass filter  $H_3(u, v)$ , where the equivalent convolution

$$\text{mask } M_3 \text{ is } M_3 = \frac{1}{9} \begin{bmatrix} 1 & 1 & 1 \\ 1 & 1 & 1 \\ 1 & 1 & 1 \end{bmatrix}.$$

Furthermore, the comb filter  $H_2(u, v)$  and its associated convolution mask  $M_2$  is the moving average filter up-sampled by the orders of  $u_x = 17$  and  $u_y = 6$ .

Therefore, the present approach involves only addition operation except in a few places. As a result, the computation effort of the present approach is only about 3% of that using the DFT and the inverse DFT such as [14].

Besides the computational advantage, the present approach also gives better inspection results. The result of the present approach is compared with that of low-pass filtering in Fig. 5. In both case, the detected defect areas are shown in grey images to avoid the effect introduced by thresholding. Please notice that, the defected areas detected by a low-pass filter [14] is seriously blurred, while the present approach gives quite sharp image of the defected area in Fig. 5(b). Due to the page length, only one set of the results are presented in this paper. However, several other images of defected LCD panels have been tested in our laboratory, in all these tests the present approach persistently shows very sharp results while the defected area detected by a low-pass filter [14] are always seriously blurred. Hence the present approach is apparently far more superior than [14].

In order to further investigate the validity of the proposed method, three more test samples are obtained from the production line, one of them is free of defects. These four samples are reproduced for 25 times each to result in 100 samples in total. These 100 samples are then tested in random sequence. The results of the present approach correctly differentiate the good sample from the three defected samples to yield a 100% of recognition rate.

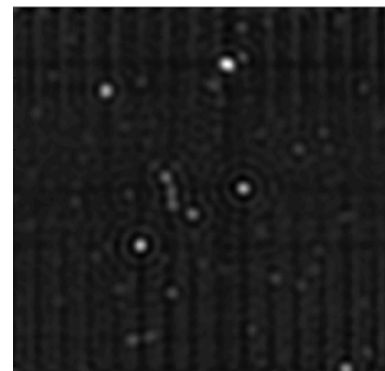
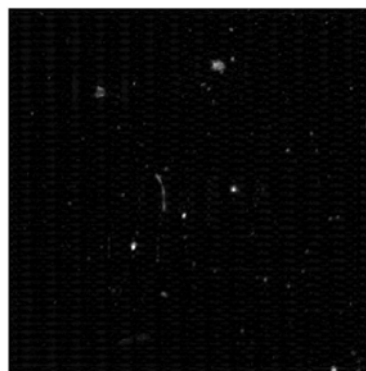
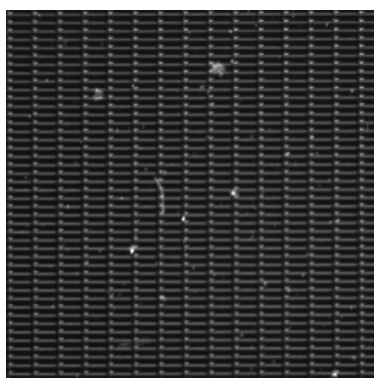
#### 4. Conclusion

A technique has been proposed for the inspection of periodic patterns using two 2-D convolution masks of the same element. The present approach is computationally efficient, and it can sharply detect the defected areas.

#### References

[1] B. E. Dom, V. H. Brecher, R. Bonner, J. S. Batchelder, and R. S. Jaffe, "The P300: A system for automatic patterned wafer inspection," *Mach Vision Appl*, vol. 1, pp. 205–221, March 1988.  
 [2] B. H. Khalaj, H. K. Aghajan, and T. Kailath, "Digital image processing techniques for patterned wafer

inspection," *SPIE Proceedings*, vol. 1926, pp. 508–516, 1993.  
 [3] S. U. Guan, P. Xie, and H. Li, "A golden-block-based self-refining scheme for repetitive patterned wafer inspections," *Mach Vision Appl*, vol. 13, pp. 314–321, 2003.  
 [4] J. Harrigan and M. Stoller, "Automated wafer inspection in the manufacturing line," *Solid State Technol.*, vol. 34, pp. 69–72, Oct. 1991.  
 [5] P. Bourgeat, F. Meriaudeau, K. W. Tobin, and P. Gorria, "Content based segmentation of patterned wafers," *J. Electronic Imaging*, vol. 13, pp. 428–435, July 2004.  
 [6] K. W. Tobin and L. Neiberg, "Metrology data management and informationsystems," in *Handbook of Silicon Semiconductor Metrology*, pp. 679–703, New York: Marcel Dekker, 2001.  
 [7] H. Y. T. Ngan, G. K. H. Pang, S.P. Yung, and M. K. Ng, "Wavelet based methods on patterned fabric defect detection," *Pattern Recognition*, vol. 38, pp. 559–576, 2005.  
 [8] A. Latif-Ameta, A. Ertuzuna, and A. Ercil, "Efficient method for texture defect detection: Sub-band domain co-occurrence matrices," *Image and Vision Computing*, vol. 18, pp. 543–553, May 2000.  
 [9] A. Bodnarova, M. Bennamoun, and S.Latham, "Optimal gabor filters for textile flaw detection," *Pattern Recognition*, vol.35, pp. 2973–2991, Dec 2002.  
 [10] A. Kumar, and G. K. H. Pang, "Defect detection in textured materials using Gabor filters," *IEEE Trans. Industry Appl.*, vol.38, pp. 425–440, March/April 2002  
 [11] C. H. Chan, and G. K. H. Pang, "Fabric defect detection by Fourier analysis," *IEEE Trans. Industry Appl.*, vol. 36, pp. 1267–1276, 2000.  
 [12] E. J. Wood, "Applying Fourier and associated transforms to pattern characterization in textiles," *Textile Res. J.*, vol. 60, pp. 212–220, 1990.  
 [13] S. A. H. Ravandi and K. Toriumi, "Fourier transform analysis of plain weave fabric appearance," *Textile Res. J.*, vol. 65, no. 11, pp. 676–683, 1995.  
 [14] Y. H. Tseng, "Automatic surface inspection for TFT-LCD array panels using Fourier reconstruction," MS thesis, Department of Industrial Engineering, Yuan-Ze University, Taiwan, 2002.  
 [15] John G. Proakis, Dimitris G. Manolakis, *Digital Signal Processing*, Prentice Hall, 1996.



(a) Original image of a LCD panel

(b) Result of the present method

(c) Result of low-pass filtering [14]

Figure 5: Defect detection of a periodic pattern